Research article

Silica/*Annona muricata* nano-hybrid: Synthesis and anticancer activity against breast cancer

Gopi Krishna Perinbarajan [a,1], Bruce Joshua Sinclair [a,1], Abdel-Tawab Mossa [b], Nupur Ohja [c], Peerzada Gh Jeelani [d,*]

[a] *Department of Biotechnology, Sri Shakthi Institute of Engineering and Technology, Coimbatore, Tamil Nadu, India*
[b] *National Research Centre, Egypt | Cairo, Egypt | NRC 33 El Buhouth St 'Ad Doqi, Dokki, Cairo Governorate, 12622, Egypt*
[c] *Department of Biotechnology, Indian Institute of Technology, Madras, Chennai, 600036, Tamil Nadu, India*
[d] *Post Graduate and Research Department of Biotechnology & Microbiology National College (Autonomous), Tiruchirapalli, Tamilnadu, 620001, India*

A B S T R A C T

Biogenically derived silica nanoparticles may serve as a well-defined target vehicle for drug delivery and have a wide range of applications in biomedicine. Silica nanoparticles are an excellent candidate as drug carriers due to their mesoporous structure, high drug loading capacity, low toxicity, environmental friendliness and low economic synthesis procedures. In this study, nano structured silica was extracted from sugarcane bagasse through an alkali leaching extraction and conjugated with *A. muricata* extract overcoming its poor solubility and improving its bioavailability within the host system. The Silica Nanoparticles (SNP) and Annona muricata conjugated Silica Nanoparticles (AM/SNP) were characterized using SEM, FTIR, TGA, EDAX, XRD and zeta potential. The AM/SNP was subjected to kinetic release studies and exhibited a sustained release of 64 % over the course of 12 h in contrast to extract, indicating the slow release of the drug under synthetic conditions. *A. muricata* pose a high affinity against tumor cells as an anti-cancer agent, and the potential of binding was testified using in-silico virtual screening against breast cancer receptors with lead acetogenins with Annomuricin (−7.4 kcal/mol) and Gigantecin (−7.4 kcal/mol) exhibiting a high binding affinity against ER and HER2+ receptors respectively. The AM/SNP conjugate exhibited high cytotoxicity against the MCF-7 breast cancer cell line with an IC50 value of 33.43 μg, indicating high potency of the conjugate at low concentrations, facilitating low systemic toxicity on administration.

1. Introduction

Natural derivatives from the plants contain phytochemicals with structural likeness contributing to the field of pharmacotherapy to fend against various diseases. In contrast to synthetic molecules, each class of phytochemicals exhibits distinct properties characterized by wide diversity and complex structural makeup. Phytochemicals possess low molecular mass, a high amount of H-bond acceptor and

---

donor, great steric complexity, and many chiral centres that grant its molecular rigidity intercepting various protein-protein interactions. It is a favoured and potential candidate in drug discovery, but its utilization is restricted due to low water solubility resulting in reduced bioavailability within the host system [1,2]. *Annona muricata (A.muricata)* is a tropical plant from the Annonaceae family known as Soursop or Graviola. *A. muricata* is widely known for its therapeutic properties and has been used within traditional medicine commodities for thousands of years. The Annonaceae family possesses a distinct class of phytochemicals termed Annonaceae Acetogenins (AGEs) that act as potent inhibitors of NADH oxidase, interrupting mitochondrial complex-1 [3]. AGEs are distinct secondary metabolites with α, β-unsaturated γ-lactone and hydroxylated tetrahydrofuran (THF) rings that support lateral diffusion within the mitochondrial membrane, inducing cytotoxic effect through altering ubiquinone reduction sites [4]. *In vivo* studies of AGEs demonstrated their antibacterial, antiviral, and anticancer properties. Despite possessing a wide range of pharmacological effects, AGEs are poorly soluble, leading to lower adsorption on oral administration [5]. It has been reported that *A. muricata* leaf extract decreased cell invasion and motility in the MDA-MB-231 cell line while causing apoptosis in the MCF-7 cell line. Thus contributing to inhibiting cell proliferation and inducing cytotoxicity among breast cancer cell lines [6]. It is also observed that various acetogenins such as annonacin, bulletin, desacetyluvaricin, and bullatalicin exhibited strong activity against different cancer cell lines expressing the potential of *A. muricata* as a lead candidate for cancer chemo preventive [7].

Breast cancer is one of the most common types of cancer, second to lung cancer worldwide. Roughly 2.3 million females were diagnosed with breast cancer around the world in 2020 and with an estimated 685,000 deaths [8]. Breast cancers are categorized into three major subtypes based on the expression of ER (estrogen), PR (Progesterone) and ERBB2 (Epidermal growth factor 2). HER2+/ERBB2-, ERBB2+ and triple-negative are major subclasses of breast cancer, with HER2+/ERBB2- the most prominent subclass with a prognosis rate over 70 %. Triple-negative breast cancers are rarer and hard to diagnose as they lack ER and PR expression, failing endocrine therapy. Chemotherapy is a widely opted method of treatment among patients with breast cancer patients, and the metastatic stage of this cancer can be treated only through chemotherapy [9]. The breast cancer cells are extremely chemo-sensitive and assist in prolonging the survival rate but have a short response duration that falls out in assuring long-term survivability against the metastatic stage. Anthracyclines and Taxanes are the most prevalent class of drugs suggested for breast cancer. It is used along with adjuvant chemotherapeutics like Trastuzumab for induced response rate, survival rate and TTP (Treatment and time of progression) [10]. Anthracyclines inhibit topoisomerase II, inducing the p53 gene-promoting transcription of Bax to repair disrupted DNA strands and promote apoptosis. The pathways of oxidative stress and apoptosis by anthracyclines are the main mechanisms contributing to the cardiac side effects. The increased ROS production leads to the loss of cardiac progenitor cells resulting in myocardial repair impairment and interacting with the structural integrity of cardiac myofibrils [11]. It has been reported that anthracyclines induce hyperthyroidism following chemotherapy with high TSH (thyroid stimulating hormone) and low fT3and fT4 levels with a prevalence of 14.8 % among 61 breast cancer patients [12]. Taxel drugs like paclitaxel and docetaxel have side effects like left ventricular dysfunction, atrioventricular block and neurotoxicity on long-term usage [13]. Hence, the discovery of a protocol for reducing toxic side effects and formulating a framework is a necessary field of research; nanotechnology, combined with biomedicine, will improve the overall technological medicine community around the globe. The Nano-medicine field involves the implementation of various nano-carriers encapsulated with Nano-sized drug particles formulated by natural or synthetic polymers. An ideal Nano-carrier poses distinct traits like targeted delivery, specificity, increased solubility, controlled release, stability and improved adsorption that enable effective delivery of the drug into the targeted site with absolute efficiency [14].

Mesoporous silica nanoparticles (MSN) have become an emerging Nano-carrier among various nanoparticles implemented in targeted drug delivery. The biogenic MSNs are characterized by porous structures enabling high drug loading capacity and controlled kinetic of drug release. The customizable particle size and pore diameter, excellent biocompatibility, and the potential functionalization of both the inner core and outer surface that assist in controlled release and targeted therapy, respectively, are the main features of MSNs [15]. MSNs can be designed and produced in a biogenic approach compared to other synthetic polymer nanoparticles. Sol-gel method is the traditional method of silica synthesis due to its ability to produce highly porous and pure silica nanoparticles at standard conditions. The chemical approach involves the formation of Nano silica in the presence of tetraethyl orthosilicate (TEOS) in an alkaline medium. Sodium silicate may serve as an alternative precursor of silica nanoparticles as it poses significant advantages over TEOS dependent sol-gel method, including homogeneous particle size coupled with highly concentrated silica nanoparticles. Agricultural wastes like coconut husk, rice husk and sugarcane bagasse are rich in silica content and serve as a potential raw source for producing sodium silicate solution-prepared silica nanoparticles. Sugarcane bagasse is commonly used as a precursor for the synthesis of silica nanoparticles due to its abundance, low cost, and eco-friendly nature. The utilization of agricultural waste materials like sugarcane bagasse helps in reducing waste accumulation and promotes sustainable practices. Sugarcane bagasse is burned as a waste disposal method, it can release smoke, particulate matter, and pollutants into the air. This can contribute to air pollution and pose health risks to nearby communities [16]. Sugarcane bagasse is discarded inappropriately, such as being dumped in water bodies or left to decompose near water sources, it can leach organic compounds and nutrients into the water. This can lead to eutrophication, algal blooms, and a decline in water quality. The silica nanoparticles derived from sugarcane bagasse have various applications in areas such as catalysis, drug delivery, sensors, and coatings [17]. In this study, we synthesize silica nanoparticles from sugarcane bagasse, thereby contributing to zero waste plans and explore the bioavailability and cytotoxic capability of a nano-conjugate developed by encapsulating A. muricata leaf extract with biogenically derived mesoporous silica nanoparticles from sugar cane bagasse ash (SBA) against breast cancer.

2. Materials and methodology

2.1. Materials

The fresh leaves of A. muricata and sugarcane bagasse were identified and collected from the Vellalur, Coimbatore district, Tamil Nadu. NaCl, KCl, Na_2HPO_4, and KH_2PO_4 were purchased from Merc life science (India), and the Sodium hydroxide, Ammonia, dialysis bag, and closure clips were purchased from HiMedia Laboratories Pvt Ltd, Mumbai, India. Whatman paper (GRADE-I, Pore size- 11 μm (Particle retention) diameter: 110 mm) was purchased from Sigma Aldrich.

2.2. Methodology

2.2.1. Extract preparation
The leaves were washed using distilled water and shade dried for 4–5 days to remove the moisture content and retain the chemical composition. Following the pretreatment, 10 g of the dried leaves of *A. muricata* were ground into a fine powder and 5 g of the powder was extraction was done traditionally using a Soxhlet apparatus with the powder being submerged under ethanol, which was used as a solvent at 80 °C and the process is done for 1 h.

2.2.2. Preparation of sugarcane bagasse ash
The Sugarcane bagasse ash (SBA) is rich in silica content, and to prepare the SBA, the Sugarcane bagasse is subjected to 1 N HCL, 1 N HNO_3, and 1 N H_2SO_4 acid treatment under 70 °C for 1 h to remove impurities and increase the silica content as reported by Norsuraya et al. [18]. The acid-pretreated samples were washed with distilled water and dried for 24 h to remove trace acidic content from the treatment. The dried bagasse was incinerated in a muffle furnace for 800° under atmospheric conditions for 4 h, producing sugarcane bagasse ash (SBA).

2.2.3. Synthesis of silica nanoparticles from SBA
For extracting silica from SBA, 100 ml of 1 N NaOH solution was stirred vigorously in the presence of 1 g of SBA under 60° overnight and filtered using Whatman paper (GRADE-I, Pore size- 11 μm (Particle retention) diameter: 110 mm) to obtain sodium silicate solution (Na_2SiO_3). At room temperature, the pH of the sodium silicate solution is brought down to 7.4 using HNO_3. The nitric acid reacts with the sodium silicate solution, forming a white silica precipitate and the solution is subjected to constant stirring for 48 h. After continuous stirring, the solution is ultra-sonicated for 1 h, breaking down the white silica precipitate and the solution is centrifuged at 10,000 rpm for 30 min. The white pellet from the centrifugation was washed multiple times with ethanol to remove all the impurities and dried in a hot air oven under 80 °C overnight. The dried Nano-silica is grounded into a fine powder using a mortar and pestle to obtain silica nanoparticles (SNP).

2.2.4. Synthesis of AM/SNP
The *Annona muricata*-conjugated silica nanoparticles (AM/SNP) were synthesized by adding 20 ml of plant extract into 100 ml sodium silicate solution. The mixture is characterized by dark green and stirred continuously for 48 h at average room temperature. After stirring, the solution was ultra-sonicated for 1 h and centrifuged at 10,000 rpm for 30 min to obtain a green precipitate of conjugated nano-silica. The precipitate was washed several times using distilled water to remove impurities and dried at 40 °C for 24 h in a hot air oven to obtain Annona muricata conjugated silica nanoparticles (AM/SNP).

2.3. Characterization of AM/SNP

2.3.1. Morphology of AM/SNP
Silica nanoparticles and AM/SNP were characterized using a Field Emission Scanning Electron Microscope (FESEM-Carl ZEISS EVO-18, Germany) Operated in both Secondary electron (SE) and Backscattered electron mode (BSD) with a resolution ranging up to 200 nm. The EDX elemental analysis was performed using an AMETEK Team V.4.3 EDS detector.

2.3.2. FTIR spectroscopy analysis
The Functional group for SNP, AM/SNP and A. muricata extract were recorded using Fourier Transform Infrared Spectroscopy carried out in a SHIMADZU miracle spectrophotometer (FTIR 820IPC). The samples were analyzed between infrared spectra ranging from 400 to 4000 cm-1 using potassium bromide (KBr) as sample carriers.

2.3.3. XRD
Utilizing Cu K radiation ($\lambda = 1.5406$), the XRD patterns of silica nanoparticles, the plant extract, and AM: SNP conjugate were examined. Measurements were made in the 2 range of 10–90° at a voltage of 40 kV and a current of 40 mA. The particle size was calculated using the Scherrer's equation ($L = K\lambda/\beta. Cos\theta$) [19].

2.3.4. Zeta potential
The zeta potential is exhibited by nanoparticles in preparation and is responsible for the inter-particle interaction. It is a physical property that measures the stability of nanoparticles and formulated drug conjugates. The zeta potential of SNP and AM/SNP were

measured using Horiba Nanopartica SZ-100 suspended in DMSO.

2.3.5. Thermogravimetric analysis (TGA)

The thermal stability of SNP and AM/SNP was determined using a Thermogravimetric analyzer (EXSTAR/6300). The nanoparticles were weighed to 1 mg and placed on an aluminum pan in a nitrogen gas environment. The temperature was gradually increased from the initial room temperature to 1000 °C, exposing the thermal resilience and weight loss at each temperature increase in the form of a graph.

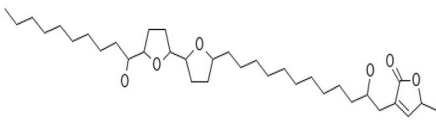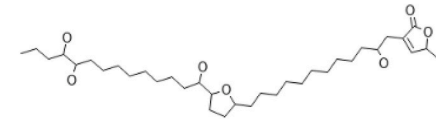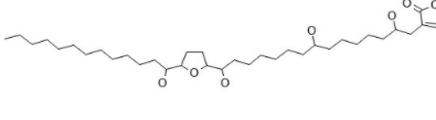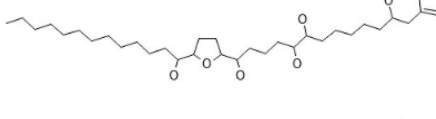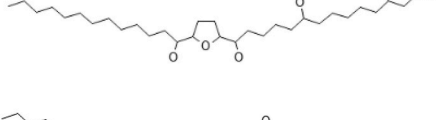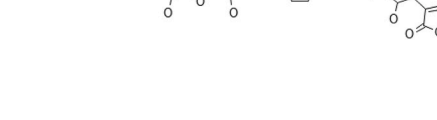### 2.4. In vitro kinetic studies

The In *vitro* kinetic-release test was performed in phosphate saline buffer (PBS) for 12 h. The phosphate saline buffer was prepared using NaCl, KCl, Na_2HPO_4, and KH_2PO_4 and adjusted to pH 7.4. AM/SNP and AM extract were dispersed in a PBS medium with the help of a dialysis membrane with a media weight cutoff of 3500 Da. The Dialysis membrane with 2 mg/ml of samples was suspended in PBS solutions and stirred for 12 h at 37 °C. At regular pre-determined intervals, 3 ml aliquots were obtained from both samples to detect the release of A. muricata into the PBS medium and 3 ml of fresh PBS was added into the medium for every aliquot taken at a particular point in time. The release was analyzed using UV-spectroscopy at a wavelength of 220 nm. The experiments were performed in triplicate, and the mean results were used to obtain the release kinetics of the AM/SNP.

2.5. In-silico analysis of A.muricata

The In-silico docking stimulation was carried out between 6 high potential acetogenins with anti-cancer properties and two protein receptor structures of breast cancer (ER and HER2+) that were obtained from RCSB Protein Data Bank (www.rcsb.org) in a PDB format (ER PDB ID: 1A52 and HER2 PDB ID: 5O4G) (Berman et al., 2000). The lead acetogenins with anti-cancer properties were selected from various literatures, as tabulated in Table 1. The ligands were prepared using CACTUS Online SMILES Translator (www.cactus.nci.nih. gov) into 3D structures for stimulations. The MGL tools developed by Scripps research institute (https://ccsb.scripps.edu/mgltools/)

Table 1
Potential Acetogenins with anti-cancer activities.

| SNo	Acetogenin	Structure	Reference
1)	Annocatacin B		[31]
2)	Annocatalin		[32]
3)	Annomutacin		[29]
4)	Annomuricin A		[30]
5)	Annonacin		[33]
6)	Gigantecin		[32]

were used to optimize protein structures by various conditions such as removing water and removing hetero atoms, the addition of Kollman charges and polar hydrogen. The energy minimization of protein and ligand structure was carried out using Swiss PBD viewer and Open Babel (http://openbabel.org/) to ensure its conformational stability in the screening process [20,21]. The Auto dock module incorporated within the Pyrx was used to dock ER and HER2+ proteins against acetogenins under full grid conditions [22].

2.6. Visualization

Discovery Studio 2021 client (https://discover.3ds.com/discovery-studio-visualizer-download) is an offline tool used to visualize the results from the virtual screening. The graphical interface of the discovery studio client visualized is a powerful tool for determining and analysing the interaction between the protein and ligands [23]. The Output PDBQT files and the protein were loaded in the discovery studio, and their 2D interaction was studied and analyzed.

2.7. MTT assay

The cancer cell line studies were carried out in the South India Textile Research Association (SITRA), Coimbatore. The samples SNP and AM/SNP were mixed in ethanol and administered to the MCF-7 cell line to assess the amount of yellow 3-(4, 5-dimethylthiazol-2-yl)-2, 5-diphenyl tetrazolium bromide (MTT) that is reduced because of activated mitochondrial succinate dehydrogenase that is present within cell cultures. The MTT solution permeates the cells and interacts with the enzymes in the mitochondria to generate a
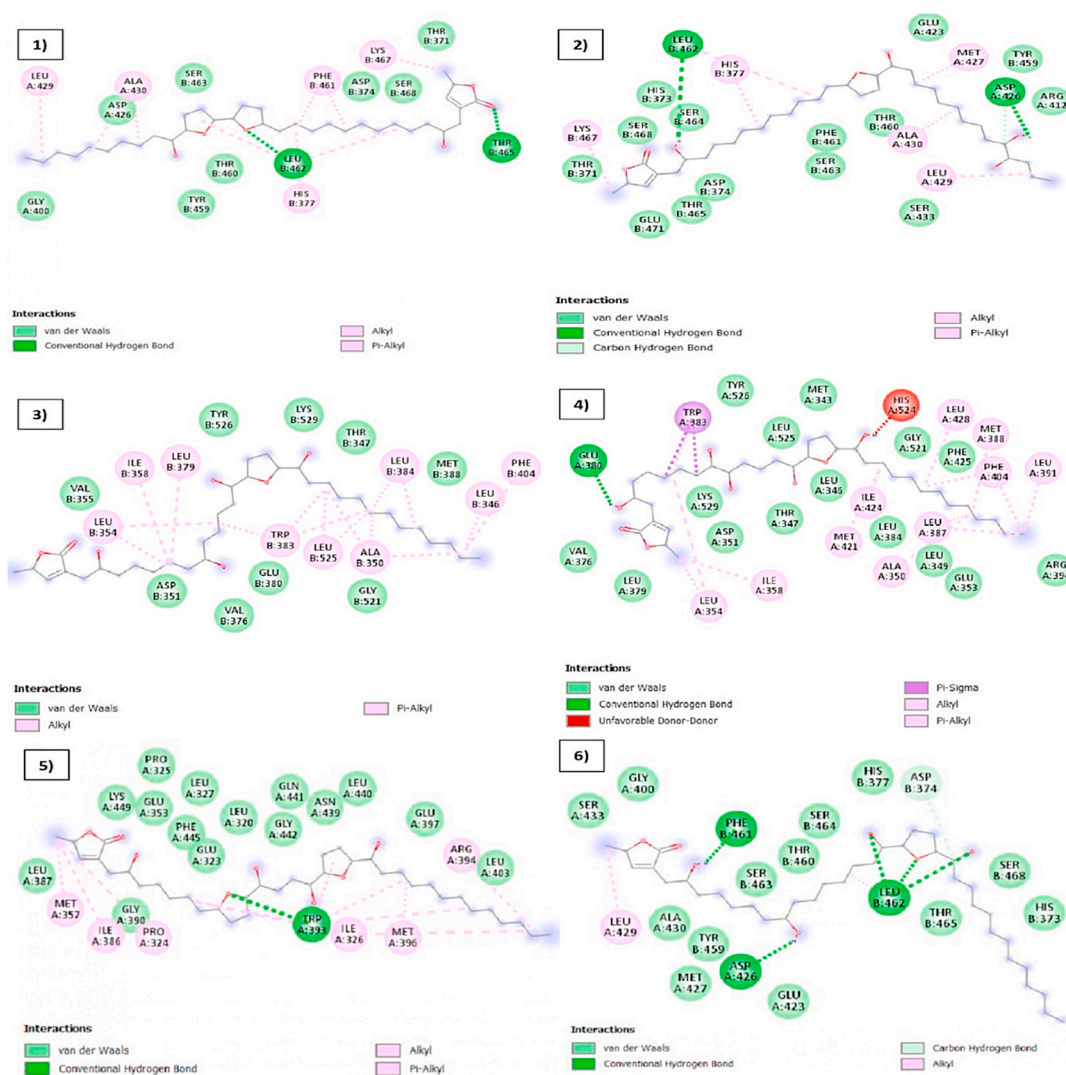
Fig. 1. Interaction of ER receptor against acetogenins 1) Annocatacin b (-6.2 kcal/mol) 2) Annocatalin (-6.5 kcal/mol) 3)Annonacin (−6.3 kcal/mol) 4) Annomuricin A (−7.4 kcal/mol) 5)Gigantecin (-6.7 kcal/mol) 6) Annomutacin (-6.1 kcal/mol).

dark purple color by facilitating the synthesis of formazan products. The formazan product is obtained and dissolved in DMSO organic solvent, and the released reagent is spectrophotometrically quantified at 570 nm over time. Test samples at various concentrations were administered to the cells, followed by incubation of the sample with cells at 37 °C for 24 h. 1 mg/ml of MTT solution was added in all the wells and incubated. The incubation process occurred in a CO_2 incubator, with a humidified atmosphere of 5 % CO_2.

Fig. 2. Interaction of HER2+ receptor against acetogenins 1) Annocatacin b (−5.5 kcal/mol) 2) Annocatalin (−4.6 kcal/mol) 3) Annonacin (−5.3 kcal/mol) 4) Annomuricin A (−5.8 kcal/mol) 5) Gigantecin (−7.4 kcal/mol) 6) Annomutacin (−6.2 kcal/mol).

3. Results and discussion

3.1. Virtual screening

The ER and HER2+ receptor proteins of breast cancer were docked against 6 high anti-cancer potential acetogenins. All 6 acetogenins exhibited strong interactions with ER and HER2+ proteins indicating the effectiveness of acetogenins against breast cancer. All acetogenins exhibited a binding affinity greater than −6.1 kcal/mol against ER protein, with Annomuricin A posing the highest binding affinity (−7.4 kcal/mol) among other ligands. Annocatacin, Annocatalin, and Annomutacin share a common hydrogen bond with LEU-462 residue. Annomuricin A form a hydrogen bond with GLU-380, and other uncommon hydrogen bond residue, including TRP-393, ASP-426, PHE-461, and THR-465. Gigantecin poses the highest binding affinity (−7.4 kcal/mol) against HER2+ protein and establishes hydrogen linkage with SER-441, THR-5, and GLN-35. Figs. 1 and 2 show that all acetogenin establishes strong hydrogen bonds and van der Waals interaction with ER and HER2+ proteins. A large amount of van der Waals interaction provides conformational stability of protein and ligand complex, contributing to the effective functioning of A. muricata against breast cancer.

3.2. Synthesis

Using the sugarcane bagasse ash, sodium silicate was prepared, and sonicated. After Sonication, the solution was stirred continuously, to obtain silica nanoparticles after centrifugation and ethanol wash. For the synthesis of AM/SNP nanoparticles, *Annona muricata* extract was mixed with sodium silicate solution and the mentioned process was repeated. After the ethanolic wash, green-coloured powder was obtained, indicating the presence of *Annona muricata* in the silica nanoparticles (Fig. 3, A-F).

3.3. Characterization

3.3.1. FTIR

The Fourier transform infrared (FTIR) transmittance spectra were taken to examine the chemical bonding of the biogenic SiO2 nanoparticles. Fig. 4, depict the FTIR results for SNP, *Annona muricata* extract and AM/SNP and shows transmission peaks ranging from 400 to 700 cm^{-1}, analogous to the rocking and symmetric bond (silanol) pulsations of the Si–O elements. The peaks spotted at 900 to 1450 cm^{-1} are correlated to the vibrational stretching of asymmetric Si–O–Si in SiO$_4$ tetrahedron, exhibiting a stoichiometric silicon dioxide (SiO$_2$) edifice. In the absorption band region, the O–H bending and O–H stretching vibration modes appeared at peaks ranging from 1500 to 1700 cm^{-1} [24]. Fig. 4, SI and AM-Sio$_2$ curves have similar peaks (especially 1064.71 and 1072.42 cm^{-1}, respectively), indicating the Si–O elements' presence. Strong absorption bands between 2884 and 3333 cm^{-1} indicate bonded –OH of alcohol or potentially –NH of amine. The absorption peaks at 2970.38 cm^{-1} could be attributed to alkane stretching vibrations, while the absorption peaks at 1664 cm^{-1} could be attributed to tertiary amides C═O stretching [25]. The peaks between 2884 and 3333 cm^{-1} in
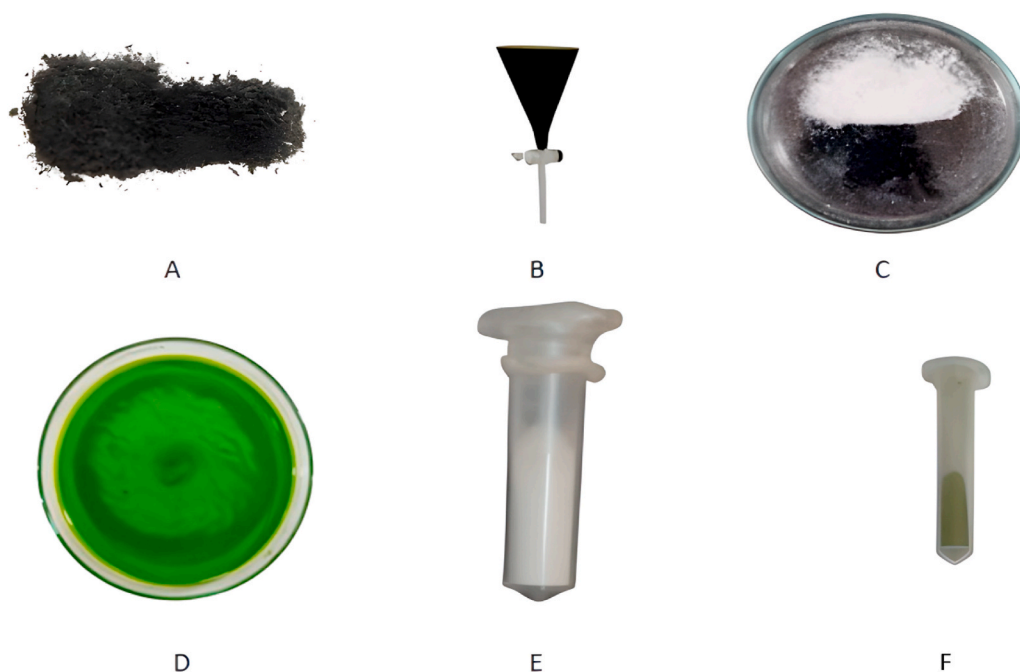

Fig. 3. Various results: (A) Sugar Bagasse Ash (B) *Annona muricata* ethanolic extract (C) Silica nanoparticles before drying (D) Conjugated nanoparticles before drying (E) SNP (F) AM/SNP.
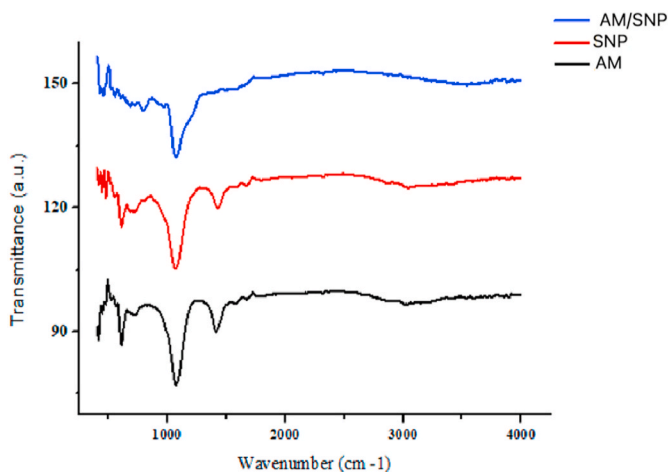
Fig. 4. FTIR analysis of (SNP) Pure Silica nanoparticles, (AM) *Annona muricata* leaf extract, indicating the presence of various compounds and alcohol and (AM/SNP) *Annona muricata* conjugated with silica nanoparticles, indicating the presence of both extract and silica.

Fig. 4 can be justified as the extract comprises ethanol. These peaks are absent in Fig. 4 a.m.-Sio_2 curve, i.e., the ethanolic content of the extract is drastically reduced during conjugation [26]. These results indicate that the *Annona muricata* has been properly conjugated with the silica nanoparticles.
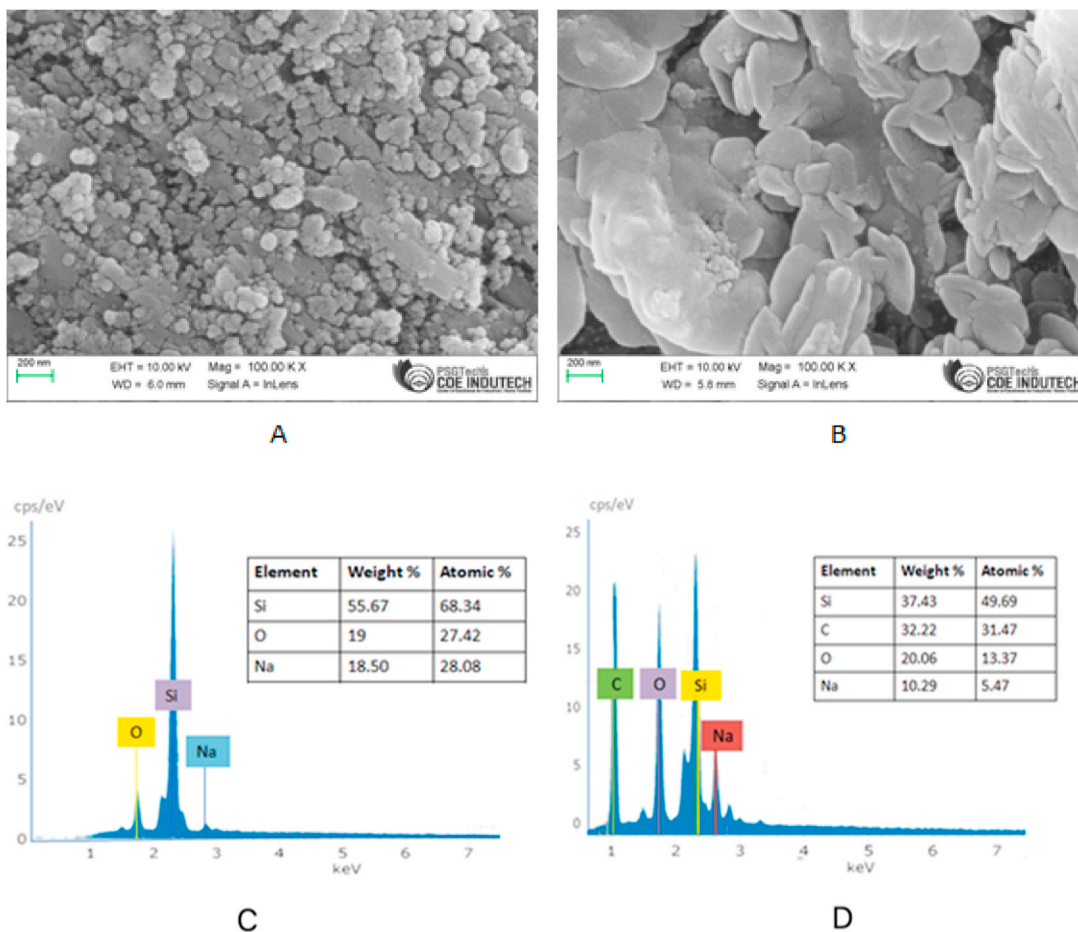
Fig. 5. SEM image of (A). Silica nanoparticles (B). AM/SNP, EDAX Analysis (C) Silica nanoparticles (D) AM/SNP indicating the amount of silica present in the prepared samples.

3.3.2. SEM and EDAX

SEM and energy-dispersive X-ray spectroscopy (EDAX) measurements were used to examine the morphological structure and elemental mapping of the SNP and AM/SNP. Fig. 5(A) and (B) show SEM images of SNP and AM/SNP, respectively. These figures were taken at a magnification of 100.00 KX. These figures show that silica nanoparticles are spherical and have a 43 ± 5 nm diameter. Fig. 5 (B) depicts silica nanoparticles as a shell surrounded by Annona muricata. Fig. 5(C) and (D) depict the Energy Dispersive X-Ray (EDAX) analysis of the silica nanoparticles and Silica: Annona muricata extract. Fig. 5(C) indicates that Silica, Sodium, and Oxygen are present in the SNP nano powder. Silica is present in a high quantity, with the percentage of weight being 55.67 %. Fig. 5(D) indicates the presence of Silica, Sodium, Carbon, and Oxygen in AM/SNP. Although silica is majorly present in AM/SNP with 37.43 %, the oxygen and carbon increase might indicate that the carboxyl groups are present in the nano powder. This indicates the presence of Annona muricata extract on the silica nanoparticles. According to Peerzada and Ramalingam's studies, along with silica and oxygen, a small amount of Sodium and carbon was present in silica nanoparticles synthesized from various agro-wastes, thereby sharing a similar result [24].

3.3.3. X-Ray Diffraction

Fig. 6 shows the X-Ray Diffraction (XRD) patterns of SNP and AM/SNP. In this pattern, the peak positions and intensities correspond to the diffraction of X-rays by the crystal lattice planes of the silica nanoparticles. In both figures, the peaks at 2θ values of approximately 20°, 28.5°, and 33.5° are characteristic of the (100), (101), and (102) planes of amorphous silica, respectively. The broadness of the peaks indicates that the silica nanoparticles are amorphous, meaning that their atoms are arranged randomly rather than in a regular, repeating lattice structure. Similar results were observed in Li et al. study [27]. The size of the nanoparticles has also been predicted using Scherrer's equation ($L = K\lambda/\beta$. Cosθ). SNP and AM/SNP calculated sizes were 39.6 nm and 46.5 nm, respectively.

3.3.4. Thermogravimetric Analysis

The thermal characteristics of the sugarcane bagasse ash were examined using a Thermogravimetric Analysis (TGA) from room temperature to 900 °C. In essence, this study gave information on the temperatures involved in pyrolysis and calcination, not the length of the procedure. Dehydration, volatilization, and carbonization are the three primary stages of their weight loss, as depicted in Fig. 7(A)–(B). Fig. 7(A) shows that the SNP do not exhibit any significant weight loss and maintain a loss level of 5 %. This slight loss is due to the removal of absorbed water and other volatile substances in SNP. Fig. 7(B) shows that The TGA curve for AM/SNP nanoparticles shows rapid weight loss in the range of 250–445 °C, which may be attributed to the degradation of Annona muricata, particularly the acetogenins present in the loaded extract. The weight loss was around 57.14 %, including the 5–10 % water and other volatile substances in AM/SNP. The TGA results show that approximately 47 % of Annona muricata gets loaded on silica nanoparticles. Jeelani and Ramalingam. have studied the TGA for Justicia adhatoda and silica nanoparticles. They had similar results; i.e., approximately 40 % of the extract was conjugated in the study [28].

3.3.5. Zeta potential

According to Fig. 8(A)–(B), the SNP's had a zeta potential of −20.8 mV, while AM/SNP had a zeta potential of −11.5 mV. Generally, the zeta potential of nanoparticles is between −10 and + 10 mV, it is said to be neutral. However, when it is larger than +30 mV or lower than −30 mV, it is said to be strongly cationic or anionic [29]. SNP has a more negative zeta potential of −20.8 mV compared to AM/SNP. This indicates that SNP has a higher surface charge density and is stable against aggregation compared to AM/SNP. This is because SNP's more substantial negative charge repels other particles with a similar charge, preventing them from coming close and forming aggregates. On the other hand, AM/SNP has a lower surface charge density (due to the conjugation), which makes it more
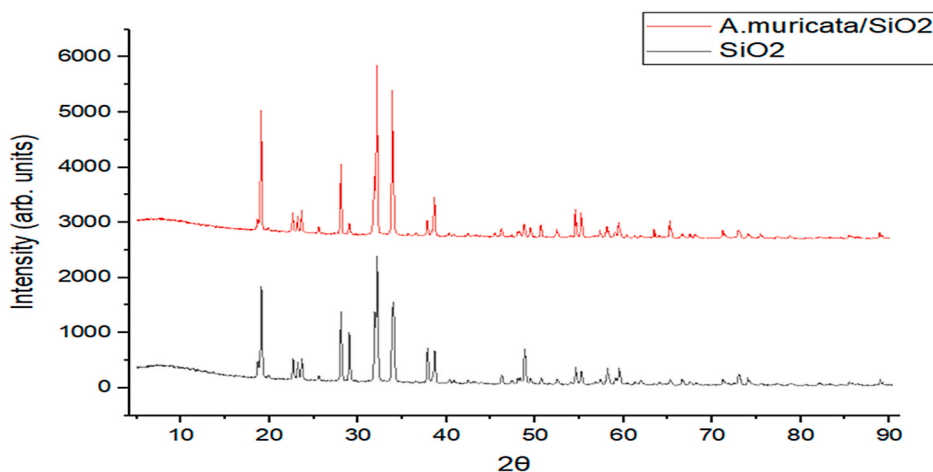

Fig. 6. XRD patterns of SNP and AM/SNP, indicating the similarities thereby confirming the presence of crystalline silica. Fig. 7: Thermogravimetric analysis of (A) SNP (B) AM/SNP.
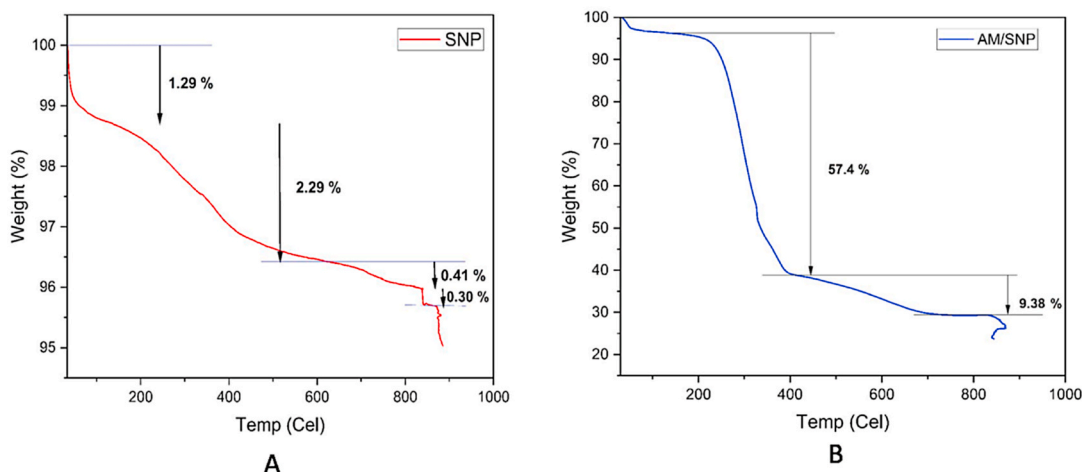
Fig. 7. Thermogravimetric analysis of SNP (A) and AM/SNP (B) respectively.
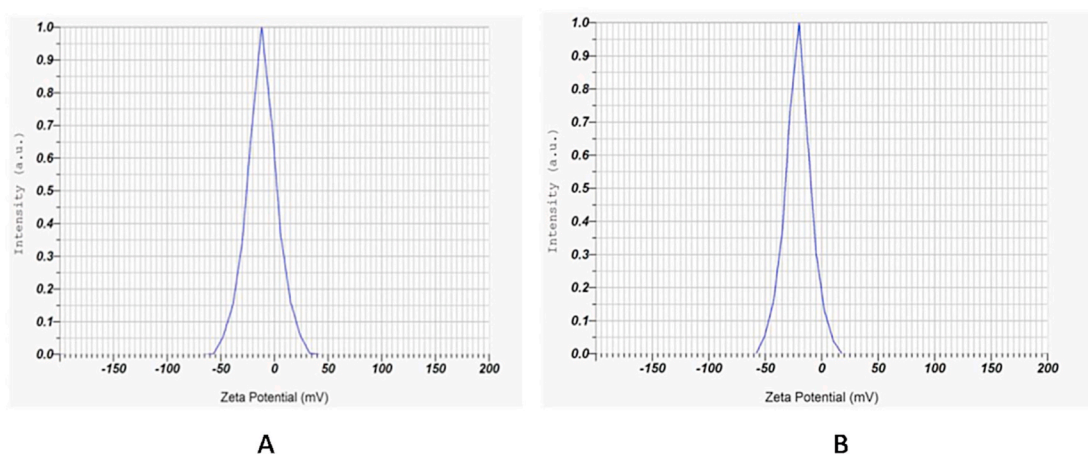

Fig. 8. Zeta potential of (A) SNP (B) AM/SNP.

prone to aggregation, as it lacks the strong repulsive forces needed to keep the particles dispersed. These numbers show that the materials' surfaces have sufficient anionic charge. According to Hamad, high values for the zeta potential were found in silica nanoparticles, which suggests that the electrostatic repulsive force that the particles are subjected to has improved their ability to disperse, while the conjugated nanoparticles' has a lower negative value due to the extract covering most of the silica's surface [30]. According to De Jong & Borm., A drug nanoparticle with extremely low negative zeta potential may be more likely to aggregate and settle, which could impair medicinal efficacy and cause significant side effects. The particles may reject one another too strongly if the zeta potential is high, preventing the particles from successfully targeting at the desired spot in the body [31]. These studies conclude that the AM/SNP is apt for drug delivery.

3.4. Kinetic release study

Using UV–vis spectroscopy, the in vitro release kinetics of AM/SNP was investigated. For the study, AM/SNP conjugate 2 mg/ml was dispersed in the phosphate buffer solution (PBS: 7.4 pH). Similarly, the extract was dissolved in PBS for the study, and the experiment was performed at 35 °C. The Maximum Absorption wavelength was set to 228 nm. The Korsmeyer-Peppas model is often used to describe drug release from polymeric systems. Fig. 9 (A) indicates the release of drug X from the polymeric matrix followed by the Korsmeyer-Peppas model with a diffusion exponent, n, of 0.140, indicating Fickian diffusion. The constant, k, was determined to be 0.230. For all samples, an initial burst release occurred in the first 1 h; however, the release magnitude of the AM-loaded samples were at least two times slower compared to the control sample (Fig. 9a). Considering the natural tendency of hydrolysis of phytochemicals compounds in water (37), the loading of phytochemicals from *Annona muricata* in silica improved its stability in water by 12 h (Fig. 9b = c). The cumulative drug release percentage for AM/SNP nanoparticles and extract was calculated. Fig. 9 (B,C) depicts the drug release has a gradual increase in AM/SNP, indicating a slow drug release, whereas a sturdy increase was observed in *Annona muricata*
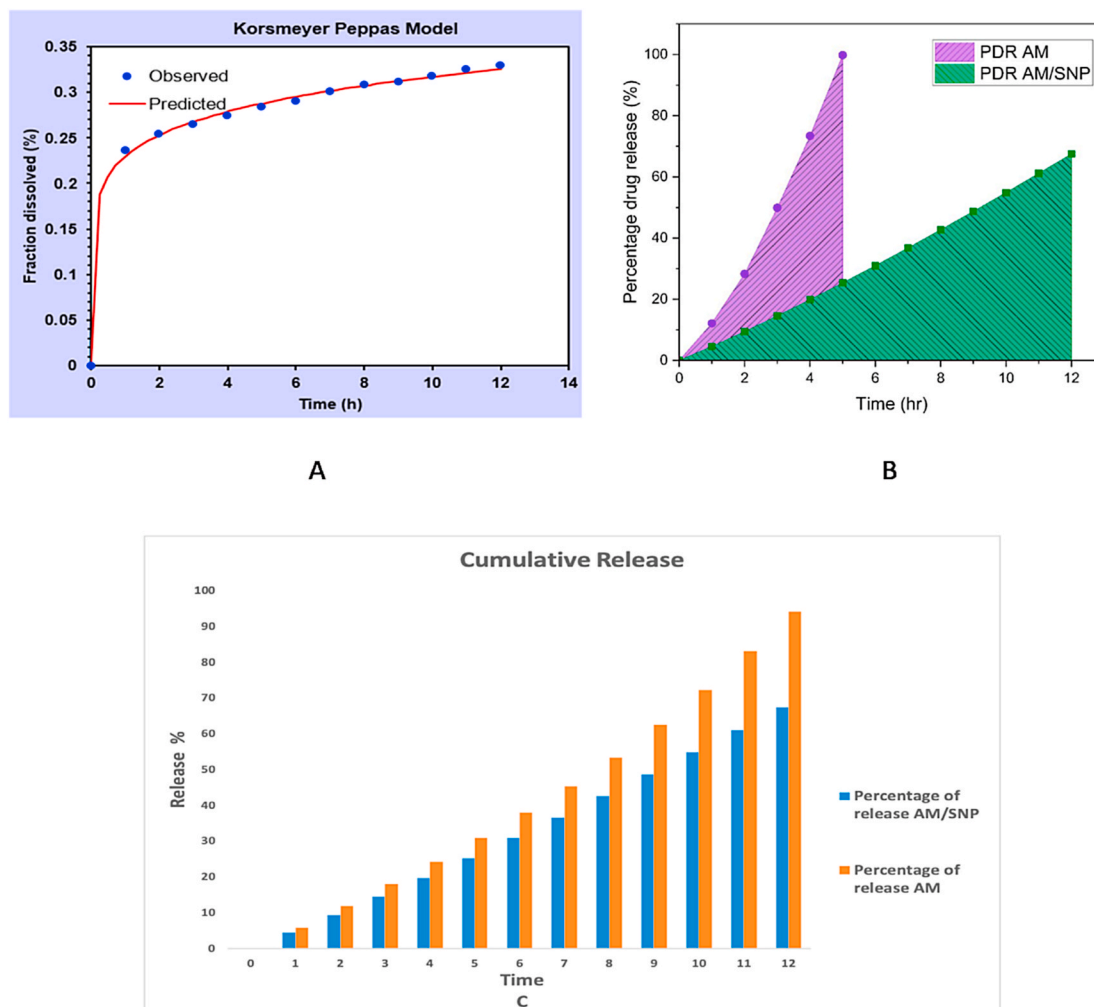
Fig. 9. Korsmeyer's model of Drug release for (A) AM/SNP (B) Percentage of Drug release of *Annona muricata* extract and AM/SNP (C) Cumulative release.

extract. At the 12th hour, the drug release for the AM/SNP was approximately 67 %, and for the Annona muricata extract was 98 % approximately. Mattos et al. reported kinetic release profile of neem bark conjugated silica nanoparticles (SiO_2/NBE), it is observed that neem bark extract release rate was lower with a release percentage of 70–80 % after 24 h which is comparatively similar to AM/SNP release profile that exhibited total release of 64 % after 12 h. In case of extract, Annona muricata release approximately 97 % of the total input to the environment within 5 h whereas neem bark extract was released completely at the end of 12th hr. The Korsmeyer model corresponds to both SiO2/NBE and AM/SNP with n values of 0.205 and 0.140, which follows controlled fickian diffusion that is responsible for slow release of the system [32].

3.5. Cytotoxicity of SNP and AM/SNP

Both SNP and AM/SNP were treated against MCF-7 to check for Anti-cancer activities. From Fig. 10(A), Cytotoxicity of SNP-treated cells on a dose-dependent concentration was found to be 15 %, 29 %, 40 %, 56 %, and 64 % increase in ROS generation at 5 μg, 25 μg, 50 μg, 75 μg, and 100 μg respectively. Whereas in the AM/SNP (Fig. 10 (B)), Cytotoxicity of the cells was 38 %, 45 %, 55 %, 72 %, and 83 % increase in ROS generation at 5 μg, 25 μg, 50 μg, 75 μg, and 100 μg, respectively. The Cytotoxicity of AM/SNP-treated cells were increased by an average of 17.8 % at every concentration compared to SNP-treated cells. The highest differences were 23 % in 5 μg and 19 % in 100 μg. From the statistical data, the toxicity of the AM/SNP was found to be significantly increased in a dose-dependent manner, compared to SNP-treated cells, which indicates that the AM/SNP treatment tends to possess the highest anti-cancer activity due to *Annona muricata* extract loaded in the nanoparticles.

In Fig. 10 (C), the Anti-proliferative assay states that in 5 μg, 25 μg SNP treated cells, dose-dependent inhibition of cell viability was observed by 85 %, 71 % compared to control, and at higher doses (75 μg, 100 μg) the cell viability found to be further decreased at a
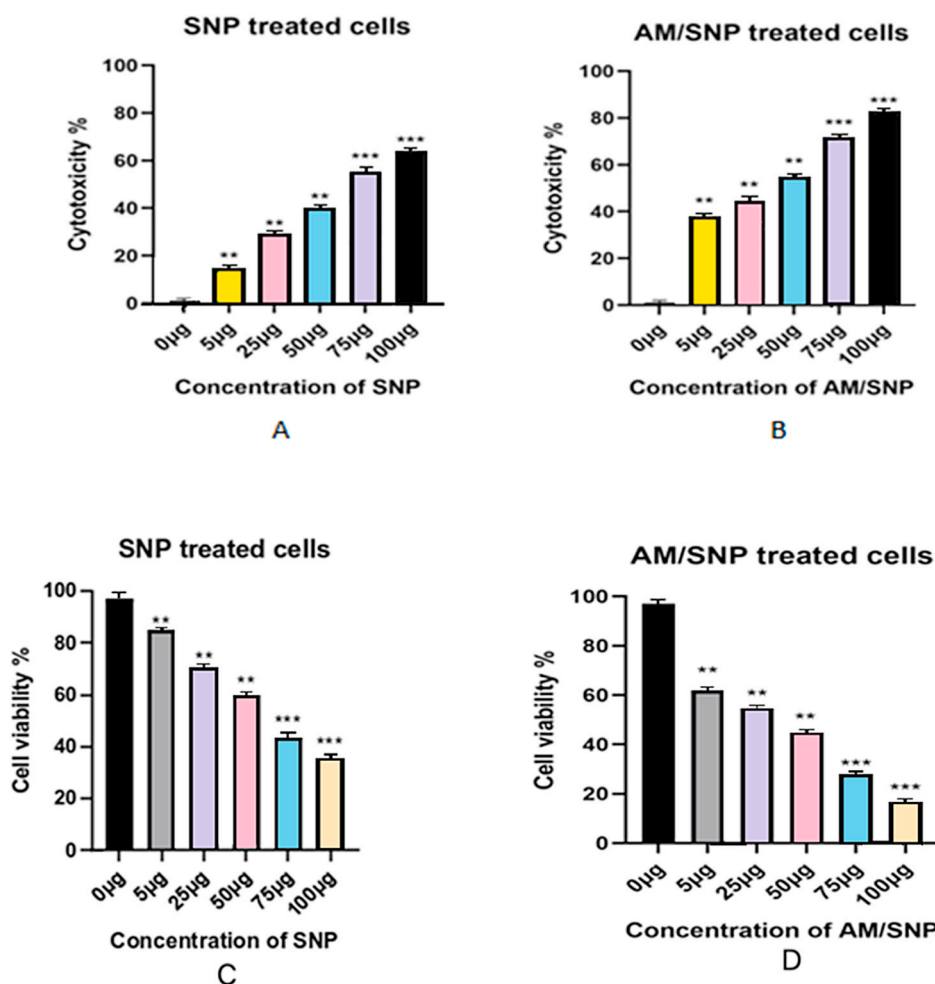
Fig. 10. (A) Cytotoxicity and Cell Viability of SNP treated and (B) Cytotoxicity of AM/SNP treated against MCF-7 cells (C) Cell viability of SNP treated and (D) Cell viability of AM/SNP treated against MCF-7 cells.

notable rate by 40 %, 36 % compared with IC50 value of 68.75 μg, Whereas in Fig. 10(D) at 5 μg, 25 μg, 50 μg treated cells the cell viability declined to 62 %, 55 %, 45 % and a further significant decrease in cell viability was observed by 17 % at 100 μg concentration with IC50 value of 33.43 μg.

Endrini et al. studied the leaf extract of Annona muricata, against breast cancer and preliminary results demonstrated that the ethanolic extract of Annona muricata leaves exhibited cytotoxic effects against MCF-7 on 24- and 48-h incubation durations, with IC50 values of 88.788 μg and 14.678 μg, respectively [33]. Cell viability gradually decreased within among increasing concentration and the IC50 value observed when the cells were treated AM/SNP is 33.43 μg. Thereby not only indicating the increase in Bioavailability of Annona muricata but also, indicating that the low concentration of AM/SNP will suffice for the anticancer activity. In Fig. 11, Apoptosis can be observed when the AM/SNP was treated against the MCF-7 cells, through Inverted Phase Contrast Microscope.

4. Conclusion

The studies showed that acetogenins present in Annona muricata have a strong binding affinity with breast cancer receptors (ER and HER2+). Acetogenins facilitate more hydrogen linkages and van der Waals interaction with the protein complex assisting in the structural stability of the overall protein-ligand complex. The structural stability and potential bond formation with various amino acid residues observed from the in-silico virtual screening testify to the potential of acetogenins as an anti-cancer agent. The conjugation of A. muricata with biogenic silica nanoparticles promises a green and non-bio accumulating slow drug release system. AM/SNP release 64 % of the total drug throughout 12 h under 37 °C. The conjugation of A. muricata with sugarcane bagasse-derived silica nano-particles promises an excellent slow drug release system under synthetic conditions with a release of 60 % over a period of 12 h under 37 °C. The slow-release system of SNP assists in improving the bioavailability of A. muricata to the targeted tumor cells, increasing the efficiency of the therapeutic agent in due course of time. TGA results showed that 47 % *A. muricata* is loaded into the silica nano-particles and exhibited high thermal stability up to 900 °C with −11.5 mV zeta potential value indicating less dispersion and more
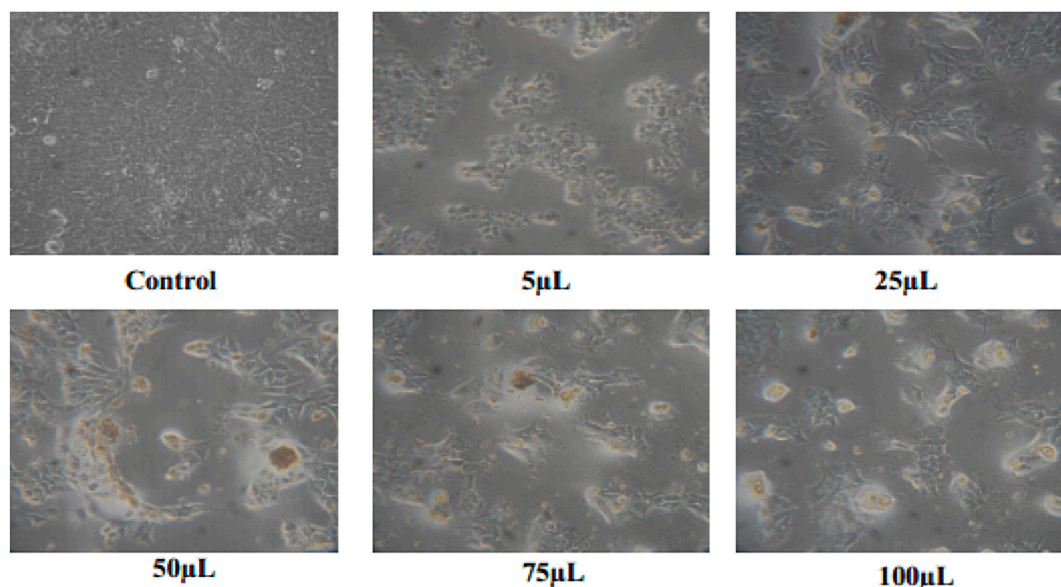
Fig. 11. Inverted Phase Contrast Microscopic images of MCF-7 cells treated with AM/SNP at different concentration.

aggregation due to surface anionic charges. The AM/SNP exhibited strong cytotoxicity against the MCF-7 breast cancer cell line with an IC50 value of 33.43 μg, indicating high toxicity in low concentration, preventing host toxic vulnerabilities on administration. The AM/SNP was found to induce Apoptosis in the MCF-7 cell line, succeeding as a potential candidate for targeted therapies against cancer. Future studies must be focused on targeting the conjugated nanoparticles toward tumor sites with increased specificity with the use of a newly composed linker and functionalizing agent that improves the overall utilization of nanoparticles as effective therapeutic agents.

Data availability statement

Data will be made available by the authors upon request.

CRediT authorship contribution statement

Gopi Krishna Perinbarajan: Writing – original draft, Visualization, Validation, Methodology, Formal analysis, Data curation, Conceptualization, **Peerzada Gh Jeelani:** Writing – review & editing, Writing – original draft, Validation, Supervision, Methodology, Investigation, Formal analysis, Data curation, Conceptualization. **Bruce Joshua Sinclair:** Writing – original draft, Validation, Resources, Methodology, Investigation, Data curation, Conceptualization. **Abdel-Tawab Mossa:** Writing – review & editing, Supervision, Conceptualization. **Nupur Ohja:** Writing – review & editing, Supervision, Investigation.

Declaration of competing interest

The authors declare that they have no known competing financial interests or personal relationships that could have appeared to influence the work reported in this paper.

Appendix A. Supplementary data

Supplementary data to this article can be found online at https://doi.org/10.1016/j.heliyon.2024.e25048.

References

[1] A.G. Atanasov, S.B. Zotchev, V.M. Dirsch, C.T. Supuran, Natural products in drug discovery: advances and opportunities, Nat. Rev. Drug Discov. 20 (3) (2021) 200–216.

[2] J. Cao, J. Cao, H. Wang, L. Chen, F. Cao, E. Su, Solubility improvement of phytochemicals using (natural) deep eutectic solvents and their bioactivity evaluation, J. Mol. Liq. 318 (2020) 113997.

[3] M.S. Patel, J.K. Patel, A review on a miracle fruits of Annona muricata, J. Pharmacogn. Phytochem. 5 (1) (2016) 137–148.

[4] K. Kuwabara, M. Takada, J. Iwata, K. Tatsumoto, K. Sakamoto, H. Iwamura, H. Miyoshi, Design syntheses and mitochondrial complex I inhibitory activity of novel acetogenin mimics, Eur. J. Biochem. 267 (9) (2000) 2538–2546.

[5] Y.J. Dang, H.Z. Feng, L. Zhang, C.H. Hu, C.Y. Zhu, In Situ Absorption in Rat Intestinal Tract of Solid Dispersion of Annonaceous Acetogenins, Gastroenterology research and practice, 2012.

[6] J.Y. Kim, T.T. Dao, K. Song, S.B. Park, H. Jang, M.K. Park, Y.S. Kim, Annona Muricata Leaf Extract Triggered Intrinsic Apoptotic Pathway to Attenuate Cancerous Features of Triple Negative Breast Cancer MDA-MB-231 Cells, Evidence-Based Complementary and Alternative Medicine, 2018.

[7] M. Mangal, M. Imran Khan, S. Mohan Agarwal, Acetogenins as potential anticancer agents, Anti Cancer Agents Med. Chem. 16 (2) (2016) 138–159.

[8] M. Arnold, E. Morgan, H. Rumgay, A. Mafra, D. Singh, M. Laversanne, I. Soerjomataram, Current and future burden of breast cancer: global statistics for 2020 and 2040, Breast 66 (2022) 15–23.

[9] A.G. Waks, E.P. Winer, Breast cancer treatment, JAMA 321 (3) (2019) 316.

[10] M.S.U. Hassan, J. Ansari, D. Spooner, S.A. Hussain, Chemotherapy for breast cancer, Oncol. Rep. 24 (5) (2010) 1121–1131.

[11] J.J. Monsuez, J.C. Charniot, N. Vignat, J.Y. Artigou, Cardiac side-effects of cancer chemotherapy, Int. J. Cardiol. 144 (1) (2010) 3–15.

[12] H. Kiyomatsu, T. Ogawa, E.I. Tsuji, N. Hayashibara, N. Yamaguchi, M. Nishio, T. Niwa, Thyroid dysfunction following conventional anthracycline-and taxane-based chemotherapy for breast cancer, Dokkyo Medical Journal 1 (3) (2022) 189–196.

[13] W.M. van den Boogaard, D.S. Komninos, W.P. Vermeij, Chemotherapy side-effects: not all DNA damage is equal, Cancers 14 (3) (2022) 627.

[14] X. Su, X. Zhang, W. Liu, X. Yang, N. An, F. Yang, H. Shang, Advances in the application of nanotechnology in reducing cardiotoxicity induced by cancer chemotherapy, Semin. Cancer Biol. 86 (2022) 929–942. Academic Press.

[15] X. Su, X. Zhang, W. Liu, X. Yang, N. An, F. Yang, H. Shang, Advances in the application of nanotechnology in reducing cardiotoxicity induced by cancer chemotherapy, Semin. Cancer Biol. 86 (2022) 929–942. Academic Press.

[16] J.S. Le Blond, S. Woskie, C.J. Horwell, B.J. Williamson, Particulate matter produced during commercial sugarcane harvesting and processing: a respiratory health hazard? Atmos. Environ. 149 (2017) 34–46.

[17] P. Sharma, J. Prakash, R. Kaushal, An insight into the green synthesis of SiO2 nanostructures as a novel adsorbent for removal of toxic water pollutants, Environ. Res. 212 (2022) 113328.

[18] S. Norsuraya, H. Fazlena, R. Norhasyimi, Sugarcane bagasse as a renewable source of silica to synthesize Santa Barbara Amorphous-15 (SBA-15), Procedia Eng. 148 (2016) 839–846.

[19] F.T.L. Muniz, M.R. Miranda, C. Morilla dos Santos, J.M. Sasaki, The Scherrer equation and the dynamical theory of X-ray diffraction, Acta Crystallogr. A: Foundations and Advances 72 (3) (2016) 385–390.

[20] N.M. O'Boyle, Banck M. James, CA Morley C. Vandermeersch T. Hutchison GR Open Babel: an open chemical toolbox, J. Cheminf. 3 (1) (2011) 33.

[21] S.P. Viewer, Kaplan W; littlejohn TG, Briefings Bioinf. 2 (2001) 195–197.

[22] S. Dallakyan, A.J. Olson, Methods in Molecular Biology, 2015.

[23] D. Studio, Discovery studio, Accelrys 2 (1) (2008).

[24] J.G. Peerzada, R. Chidambaram, A statistical approach for biogenic synthesis of nano-silica from different agro-wastes, Silicon 13 (2021) 2089–2101.

[25] S.A. Akintelu, A.S. Folorunso, Characterization and antimicrobial investigation of synthesized silver nanoparticles from Annona muricata leaf extracts, J Nanotechnol Nanomed Nanobiotechnol 6 (2019) 1–5.

[26] A. Monshi, M.R. Foroughi, M.R. Monshi, Modified Scherrer equation to estimate more accurately nano-crystallite size using XRD, World J. Nano Sci. Eng. 2 (3) (2012) 154–160.

[27] P. Li, X. Zhang, J. Shen, Synthesis and characterization of mesoporous silica nanoparticles, Microporous Mesoporous Mater. 117 (1–2) (2009) 428–433.

[28] P.G. Jeelani, C. Ramalingam, Statistical approach to synthesise biogenic silica nanoparticles from rice husk and conjugated with Justicia adhatoda extract as green, slow-release biocide, IET Nanobiotechnol. 15 (4) (2021) 391–401.

[29] J.D. Clogston, A.K. Patri, Zeta potential measurement, Methods Mol. Biol. 697 (2011) 63–70, https://doi.org/10.1007/978-1-60327-198-1_6. PMID: 21116954.

[30] B.A. Hamad, M. Xu, W. Liu, Performance of environmentally friendly silica nanoparticles-enhanced drilling mud from sugarcane bagasse, Part. Sci. Technol. 39 (2) (2021) 168–179.

[31] D.W.H. Jong, P.J.A. Borm, Drug delivery and nanoparticles: applications and hazards, Int. J. Nanomed. 3 (2008) 133–149.

[32] B.D. Mattos, O.J. Rojas, W.L. Magalhães, Biogenic silica nanoparticles loaded with neem bark extract as green, slow-release biocide, J. Clean. Prod. 142 (2017) 4206–4213.

[33] S. Endrini, S. Suherman, W. Widowati, *Annona muricata* leaves have strongest cytotoxic activity against breast cancer cells, UniversaMedicina 33 (3) (2014) 179–184.